water

MDPI

Article

Effects of Drying Operation on the Mn^{2+} Removal Activity of MnO_x: Performance and Mechanism

Ruifeng Zhang [1,2,*], Lina Yang [1], Jing Yang [1], Qiuyan Niu [1] and Binrong Zhu [1]

[1] School of Urban Planning and Municipal Engineering, Xi'an Polytechnic University, Xi'an 710048, China; yanglina1128@163.com (L.Y.); jingy76@163.com (J.Y.); niu091824@163.com (Q.N.); 16623403654@163.com (B.Z.)
[2] Key Laboratory of Membrane Separation of Shaanxi Province, Xi'an University of Architecture and Technology, Xi'an 710055, China
* Correspondence: ruifengzhangtry@xpu.edu.cn

Abstract: Mn^{2+} is a prevalent contaminant in groundwater. In this study, manganese oxides (MnO_x) were prepared via a redox method to remove Mn^{2+} from water. The effects of the drying operation in the preparation process, including heat drying at 20–120 °C with different times and freeze drying methods, on the structural properties, manganese removal performance and mechanisms were investigated. The results indicate that the drying conditions can significantly affect the removal performance and stability of MnO_x. The MnO_x dried at 50 °C for 12 h exhibited the best Mn^{2+} removal efficiency and stability, with an adsorption capacity of 125.7 mg/g and removal efficacy of 95.1% after six reuse cycles. The removal pathway experiments revealed that the sample dried at 50 °C for 12 h had superior catalytic oxidation abilities for Mn^{2+}, while other samples removed Mn^{2+} by primarily relying on the adsorption process. The investigation of the structure revealed that excessive heat drying led to the shrinkage of the oxide particles, a reduction in the surface voids, and a decrease in the hydroxyl groups. Conversely, insufficient drying time or temperatures resulted in high water content in MnO_x, which occupied the surface active sites. The XPS analysis indicated that the catalytic oxidation of Mn^{2+} primarily relied on Mn(III) and adsorbed oxygen on the surface of MnO_x. With freeze drying or inadequate heat drying, a large amount of Mn(II) remained on the oxide surface, and the over-drying operation resulted in excessive conversion from Mn(II) to Mn(IV), reducing the catalytic activity and resulting in low removal stability.

Keywords: manganese oxides; manganese removal; drying operation; adsorption; catalytic oxidation

Academic Editor: Chengyun Zhou

Received: 2 December 2024
Revised: 15 January 2025
Accepted: 15 January 2025
Published: 17 January 2025

Citation: Zhang, R.; Yang, L.; Yang, J.; Niu, Q.; Zhu, B. Effects of Drying Operation on the Mn^{2+} Removal Activity of MnO_x: Performance and Mechanism. *Water* **2025**, *17*, 261. https://doi.org/10.3390/w17020261

1. Introduction

Groundwater is an important drinking water source in China [1]. Manganese contamination is a prevalent issue in groundwater, leading to various sensory and operational challenges, such as discoloration, laundry stains, and pipe clogging [2]. Moreover, it also poses significant health risks [3], including chronic poisoning, abnormal neurological function, and endocrine dysfunction [4]. In nature, manganese is widely found in igneous and sedimentary rocks, and it can be dissolved into groundwater [5]. When groundwater flows through the soil and rocks, the concentration of manganese will be naturally elevated, due to the weathering and leaching of manganese-containing minerals [6]. Additionally, manganese can also come from human activities, such as industrial emissions, mining and mineral processing, and waste landfills [7]. Industrial wastewater containing manganese may be directly discharged into water bodies, resulting in serious manganese pollution

accidents in aquatic environments [5]. Moreover, manganese can enter aquifers via the leaching solutions and runoff from mining, solid waste, and landfills [8].

At present, manganese contamination is becoming a growing issue due to the increasing demand for materials containing manganese, such as steel products and batteries [7]. Moreover, self-purification and restoration are almost impossible once contamination occurs, due to the lengthy natural renewal cycle of groundwater, making the issue more serious [9]. Therefore, the effective removal of manganese from groundwater remains a critical challenge in drinking water treatment [10].

Several methods are employed for the removal of manganese from drinking water, including chemical reagent oxidation, adsorption methods, biological processes, and chemical catalytic oxidation [11,12]. Among these, the utilization of manganese oxides as adsorbents or catalysts is a particularly promising approach [13]. Manganese oxides are abundantly present in the Earth's crust [13]. They possess a strong affinity for metal ions and can efficiently remove Mn^{2+} from water due to their large specific surface area, abundant micropores, and high reactivity [14].

MnO_x can be utilized either as powder materials or as coatings on various filter media, such as quartz sand, zeolite, and activated carbon [3,6], and it also plays crucial roles in chemical reagent oxidation and biological processes [14,15]. The removal of Mn^{2+} by manganese oxides occurs primarily through adsorption and catalytic oxidation pathways simultaneously. The removal efficiency and mechanisms of Mn^{2+} by MnO_x are commonly influenced by the surface morphology, the valence state of Mn, and the species of reactive oxygen [16]. It has been proven that Mn^{2+} can react with the surface hydroxyl groups to form a hydroxyl complex connected by a coordination bond [17]. Additionally, structural defects are also an effective way to improve the adsorption capacity [18]. For example, oxygen vacancies are found to be capture centers, which are conducive to the adsorption of inorganic ions [19]. It has been known that Mn(III) has high reactivity and can promote the oxidation of Mn^{2+} [20]. According to the theory of catalytic oxidation, the removal process involves rapid adsorption followed by relatively slow catalytic oxidation, as described in Equations (1) and (2) [21].

$$Mn^{2+} + MnO_2 \cdot xH_2O(s) \rightarrow MnO_2 \cdot MnO \cdot (x-1)H_2O(s) + 2H^+ \quad (1)$$

$$MnO_2 \cdot MnO \cdot (x-1)H_2O(s) + \frac{1}{2}O_2 + H_2O \rightarrow 2MnO_2 \cdot xH_2O(s) \quad (2)$$

Initially, Mn^{2+} is adsorbed onto the active surface sites of MnO_x; subsequently, MnO_x facilitates the efficient utilization of dissolved oxygen to oxidize the adsorbed Mn^{2+}, converting it back into MnO_x and regenerating the active sites in the process [22]. Our previous studies have investigated the impact of structural cations on the activity of MnO_x, revealing that Ca^{2+} doping can enhance Mn^{2+} removal more effectively than Na^+, K^+, and Mg^{2+}.

Additionally, manganese oxides commonly contain large amounts of surface-adsorbed water and structural water [23]. The amount and behavior of this water are closely related to the ambient temperature and the valence state of manganese, significantly impacting the Mn^{2+} removal performance and mechanism [24]. Drying operations are commonly employed to control the water content and species in the preparation process of MnO_x, and it can also induce some changes in the structure [25]. It was observed that the catalytic activity and stability of electrodeposited manganese oxide were slightly improved following heat treatment at 90 °C for 2 h [26]. Conversely, the loss of interlayer water molecules during natural drying was found to negatively affect the catalytic activity of Fe-Mn co-oxides [27]. Although drying operations are crucial in the preparation of MnO_x, their effects on the Mn^{2+} removal activity of MnO_x and the corresponding underlying mechanisms are still unclear, and there is little research that addresses this problem.

The aim of this study was to investigate the effects of the drying operation on the water properties, structural changes, and Mn^{2+} removal performance of MnO_x. Moreover, the corresponding influence mechanism of the drying operation was investigated. The results will help to select appropriate drying operations in the preparation of high-reactivity MnO_x and further elaborate on the removal mechanism of Mn^{2+}.

2. Materials and Methods

2.1. Preparation of MnO_x

First, 10.08 mL of 0.3 mol/L $KMnO_4$ solution was slowly added to 10.2 mL of 0.1 mol/L $CaCl_2$ and 6% $MnCl_2$ solution. After the reaction was finished, the suspension was filtrated to obtain MnO_x particles. The prepared particles were washed with deionized water several times until the pH of the cleaning water was approximately 7.0. Then, the obtained MnO_x was placed in an oven or a vacuum freeze dryer and dried with different drying operations. Finally, the dried MnO_x was kept in a sealed container before use.

2.2. Characterization of MnO_x

The morphology of MnO_x was characterized by scanning electron microscopy (SEM, Quanta FEG 250, FEI, Hillsborough, OR, USA). XRD patterns were recorded by an X-ray diffractometer (XRD, UltimalV, Rigaku, Tokyo, Japan) with Cu Kα radiation (λ = 0.1542 nm) and a tube voltage of 40 kV. Continuowere taken in a 2θ range of 5–80° with a scan rate of 5° min^{-1} and a step size of 0.02°. X-ray photoelectron spectroscopy (XPS) was performed using a photoelectron spectrometer (Thermo Scientific K-Alpha, Waltham, MA, USA) equipped with a monochromatic Al Kα excitation source. The binding energies were calibrated using the C1s binding energy at 284.6 eV. FTIR spectra were detected by a Fourier transform infrared spectrometer (Thermo Fisher Nicolet IS5, Waltham, MA, USA); the FTIR spectra of MnO_x under different drying conditions were detected in the range of 4000–400 cm^{-1} with a resolution of 0.16 cm^{-1}. Thermogravimetric–differential thermal analysis (HTC-4, Hengjiu, Bejing, China) was determined in the temperature range of 25 to 600 °C with a heating rate of 10 °C/min under flowing dry air.

2.3. Evaluation of Removal Capacity and Mechanism

2.3.1. Adsorption Models

Experiments on the isothermal adsorption and adsorption kinetics were carried out on a magnetic stirrer. The temperature was 25 °C, and the amount of added manganese oxides was 0.2 g/L. The reaction solution was a mixture of $MnCl_2$ and $NaHCO_3$. As the pH can significantly influence the adsorption behavior of MnO_x, $NaHCO_3$ of 200 mg/L was added into the reaction solution to maintain the pH within the range of 7.9–8.3 in the Mn^{2+} removal process. The concentration of Mn^{2+} in the isothermal adsorption and adsorption kinetics experiments was 15–90 mg/L and 25 mg/L, respectively. Samples of 5 mL were taken at 5, 10, 20, 30, 60, 90, 150, and 300 min and were filtered through 0.22 μm filter membranes to determine the concentration of Mn^{2+}.

Pseudo-first- and second-order kinetics were used to analyze the adsorption process of Mn^{2+} on MnO_x. The adsorption kinetics models and their equations are shown in Equations (3) and (4). The pseudo-first-order kinetics is as follows:

$$\log(q_e - q_t) = \log q_e - \frac{k_1}{2.303} t \quad (3)$$

where q_e is the adsorption capacity at equilibrium, mg/g; q_t is the adsorption capacity at time t, mg/g; t is the adsorption time, h; and k_1 is the equilibrium constant, 1/min. The pseudo-second-order kinetics is as follows:

$$\frac{t}{q_t} = \frac{1}{k_2 {q_e}^2} + \frac{1}{q_e} t \quad (4)$$

where k_2 is the relative equilibrium constant, 1/min.

The adsorption isotherm model is a crucial tool in evaluating the adsorption capacities and characteristics of adsorbents. Commonly used theoretical models include the Langmuir and Freundlich isotherm models. The Langmuir isotherm model is based on several key assumptions, such as that the adsorbent surface is homogeneous, all adsorption sites have identical energies, and adsorption occurs in a monomolecular layer, etc. [28]. The model is described as in Equation (5):

$$q_e = \frac{q_{max} K_L C_e}{1 + K_L C_e} \quad (5)$$

where q_{max} is the maximum adsorption capacity, mg/g; K_L represents the adsorption equilibrium constant; and C_e corresponds to the fluoride ion concentration after equilibrium, mg/L.

The Freundlich isothermal model applies to both monolayer adsorption (chemisorption) and multilayer adsorption (physisorption); it is based on the fact that the adsorption process occurs on the inhomogeneous surface of the adsorbent [29]. The equation is shown in Equation (6):

$$q_e = K_F \cdot {C_e}^{\frac{1}{n}} \quad (6)$$

where n is the adsorption constant; K_F is the adsorption equilibrium constant.

The adsorption constant n is affected by the temperature, and, when n < 0.5, the adsorption process is considered to be difficult. When n = 2–10, the adsorption process can proceed easily [30]. The value of 1/n is related to the adsorption kinetic force and adsorption potential energy, and the smaller the value, the stronger the adsorption strength and the heterogeneity of the adsorbent surface [31].

2.3.2. Stability and Applicability Experiments

Manganese oxide of 0.2 g/L was added into a beaker and dispersed with pure water by ultrasonication. Then, the suspension was mixed with a certain amount of $MnCl_2/NaHCO_3$ solution. The concentrations of Mn^{2+} and $NaHCO_3$ were 5 mg/L and 200 mg/L, respectively, and the volume of the reaction solution was 1 L. After this, the beaker was placed on a magnetic stirrer to carry out the reaction at a temperature of 25 °C. One reaction cycle was 300 min. Samples of 5 mL were taken at 5, 10, 20, 30, 60, 90, 150, and 300 min and were filtered through 0.22 μm filters to determine the concentration of Mn^{2+}. After one cycle was completed, the reaction solution was filtered to separate MnO_x and then the separated MnO_x was cleaned several times using deionized water. Finally, the MnO_x was used again in the next cycle. A total of 6–8 cycles were processed in this experiment.

To elaborate on the applicability of MnO_x, tap water from groundwater sources was used to simulate real conditions. The MnO_x treated at 50 °C for 12 h was coated on quartz sand and a dynamic filtration test was conducted, as reported in a previous study, to evaluate the applicability of MnO_x [32]. Firstly, quartz sand with a particle size of 0.5–2.0 mm was soaked in 1 mol/L HCl for 24 h and then washed with deionized water to neutral and dried at 105 °C for backup use. Secondly, 500 g of acid-modified quartz sand was thoroughly mixed with a solution of 51 mL containing 0.1 mol/L $CaCl_2$ and 6%

$MnCl_2$, and then 0.3 mol/L $KMnO_4$ of 50.4 mL was slowly added. After the reaction was completed, the sands were dried at 50 °C for 12 h to obtain MnO_x filter material. Finally, the filter material was filled into a plexiglass column with an inner diameter of 50 mm. The depth of the filter material was 1000 mm. Sampling ports were set at every 200 mm along the height of the filter material. The filtration rates and the Mn^{2+} concentration in the influent water of the filter were in the range of 6–12 m/h and 0.3–1.0 mg/L, respectively. Besides the concentration of Mn^{2+}, all water parameters are shown in Table 1.

Table 1. Water quality of the influent water for the filter column.

Parameter	Unit	Value
Temperature	°C	10.0–20.0
Dissolved oxygen concentration	mg/L	7.40–8.10
pH value	/	7.61–8.23
Turbidity	NTU	0.12–0.34
CODMn	mg/L	0.90–1.50
TOC	mg/L	0.69–3.97
Alkalinity (as CaCO3)	mg/L	135.28–137.52

2.3.3. Effects of Oxygen

The effects of oxygen on Mn^{2+} removal were investigated by the method reported in a previous study, with a minor modification [33]. A $MnCl_2/NaHCO_3$ solution of 1 L was added into a flat-bottomed flask. The concentrations of $NaHCO_3$ and Mn^{2+} in the solution were 200 mg/L and 0.2 g/L, respectively. Then, 0.2 g of MnO_x was added to the above solution to carry out the reaction. In the experiment, air or N_2 was continuously poured into the reactor with a certain flow rate, and the pH of the solution was adjusted with 1 M HCl and NaOH to keep the pH maintained at about 8.5. Samples of 5 mL were taken out at certain time intervals (0.5 h, 1.0 h, 2.0 h, 5.0 h, 8.0 h, 11.0 h, 14.0 h, 24.0 h) and filtrated with a 0.22 μm filter membrane, and the Mn^{2+} concentration was determined.

2.4. Analytical Methods

The chemical reagents used in the experiments were purchased from Sinopharm Chemical Reagent Co., Ltd. (Shanghai, China). The reagents were all of analytical grade and used without further purification. The pH and dissolved oxygen (DO) were measured using a precision acidity meter (PHS-3 C, Leici Co., Ltd., Shanghai, China) and a dissolved oxygen meter (JPB-607A, Leici Co., Ltd., Shanghai, China), respectively. The concentrations of Mn^{2+} were measured by potassium periodate oxidation spectrophotometry according to the guidelines of the Ministry of Environmental Protection of China.

3. Results and Discussion

3.1. Removal Performance of Mn^{2+}

The removal performance of Mn^{2+} by MnO_x treated under different drying conditions is shown in Figure 1. It can be seen that when the drying time increased from 1 h to 12 h, the Mn^{2+} removal efficiency of MnO_x increased obviously, and the maximum removal rate of Mn^{2+} at the reaction time of 300 min was up to 99.6% (Figure 1a). However, extending the drying time to 24 h resulted in a reduction in the Mn^{2+} removal efficiency. The effect of the drying temperature on the Mn^{2+} removal is shown in Figure 1b. When the drying temperature increased from 20 °C to 50 °C, the Mn^{2+} removal efficiency increased. As we continued to increase the temperature, the Mn^{2+} removal efficiency began to decline, and the removal efficiency of the sample dried at 120 °C was the lowest. Additionally, the Mn^{2+} removal rate of the 12 h freeze-dried MnO_x was comparable to that of the MnO_x dried

at 20 °C or 80 °C. When the drying temperature is low or the drying time is short, more adsorbed water will remain on the surface of MnO_x. Excessive adsorbed water can lead to a decrease in the number of reactive sites [34], resulting in a relatively low Mn^{2+} removal rate by MnO_x. However, when the drying temperature is too high or the drying time is too long, there may be a change in the structure of MnO_x [35]. Thus, there exist optimal drying conditions for MnO_x to obtain the maximum Mn^{2+} removal efficiency.

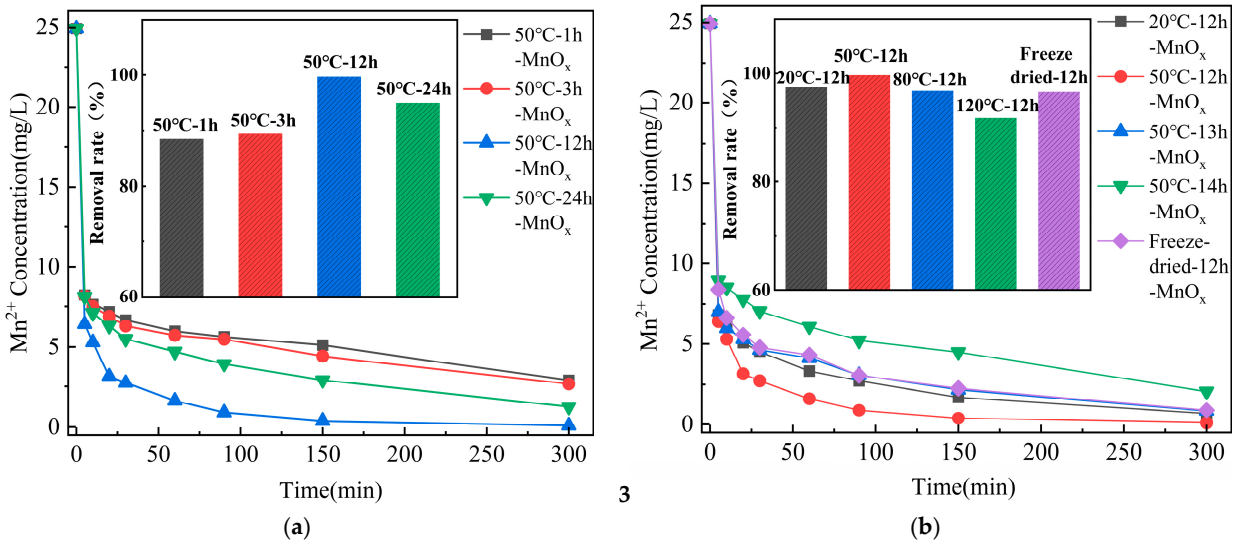

Figure 1. The removal performance of Mn^{2+} by MnO_x dried at different (**a**) times and (**b**) temperatures.

3.2. Adsorption Kinetics

The kinetic fitting results are shown in Figure 2a,b and Table 2. Both pseudo-first-order and pseudo-second-order kinetic models can effectively describe the adsorption process. The correlation coefficients (R^2) for both models are greater than 0.99, with the pseudo-second-order model providing a superior fit. The pseudo-second-order model assumes that the adsorption process is governed by chemical adsorption [36], suggesting that the adsorption of Mn^{2+} involves a chemical adsorption process. In addition, the highest adsorption capacity was obtained by 50 °C-12 h-MnO_x, with a q_e of 125.7 mg/g.

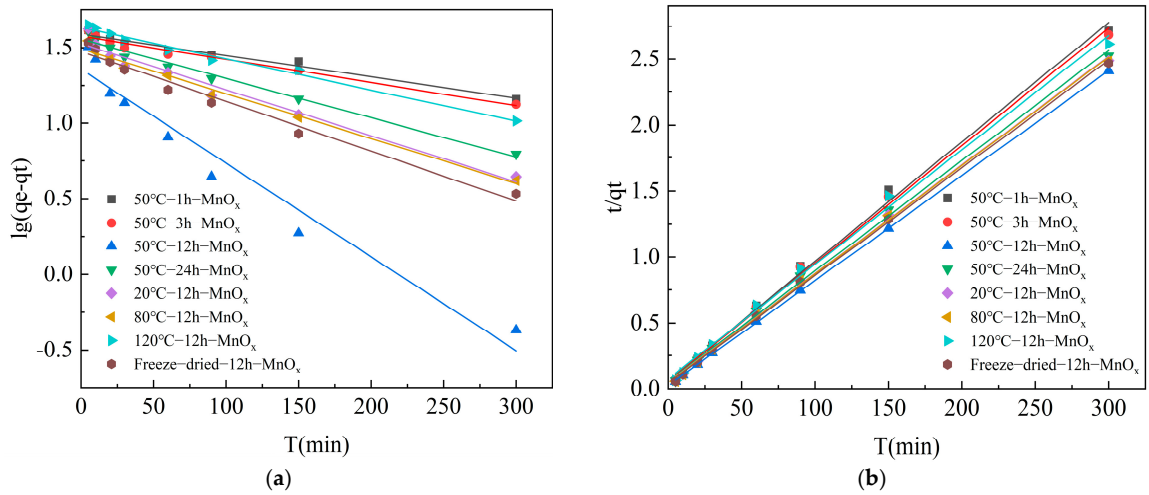

Figure 2. Adsorption kinetics of Mn^{2+} by MnO_x under different drying conditions: (**a**) pseudo-first order kinetic plots and (**b**) pseudo-second order kinetic plots (MnO_x = 0.2 g/L, Mn^{2+} = 25 mg/L, T = 25 °C, t = 300 min).

Table 2. Kinetic parameters of Mn^{2+} adsorption by MnO_x under different drying conditions.

Sample	Pseudo-First-Order			Pseudo-Second-Order		
	K_1 (min^{-1})	q_e (mg/g)	R_1^2	K_2 ($g \cdot mg^{-1} \cdot min^{-1}$)	q_e (mg/g)	R_2^2
50 °C-1 h-MnO_x	0.0032	38.74	0.969	0.0013	110.5	0.996
50 °C-3 h-MnO_x	0.0035	37.59	0.972	0.0014	111.2	0.997
50 °C-12 h-MnO_x	0.0142	22.68	0.949	0.0025	125.7	0.999
50 °C-24 h-MnO_x	0.0059	35.99	0.980	0.0012	119.6	0.997
20 °C-12 h-MnO_x	0.0070	33.61	0.960	0.0013	121.5	0.998
80 °C-12 h-MnO_x	0.0068	31.39	0.984	0.0014	121.6	0.998
120 °C-12 h-MnO_x	0.0070	41.83	0.984	0.0010	115.2	0.995
Freeze-dried-12 h-MnO_x	0.0076	29.81	0.972	0.0015	122.5	0.999

3.3. Adsorption Isotherms

The adsorption isotherms of Mn^{2+} by MnO_x are shown in Figure 3, and the corresponding isothermal adsorption fitting results are shown in Table 3. As shown in Figure 3a, the Langmuir model cannot fit the adsorption process well. Therefore, the relative parameters were not calculated.

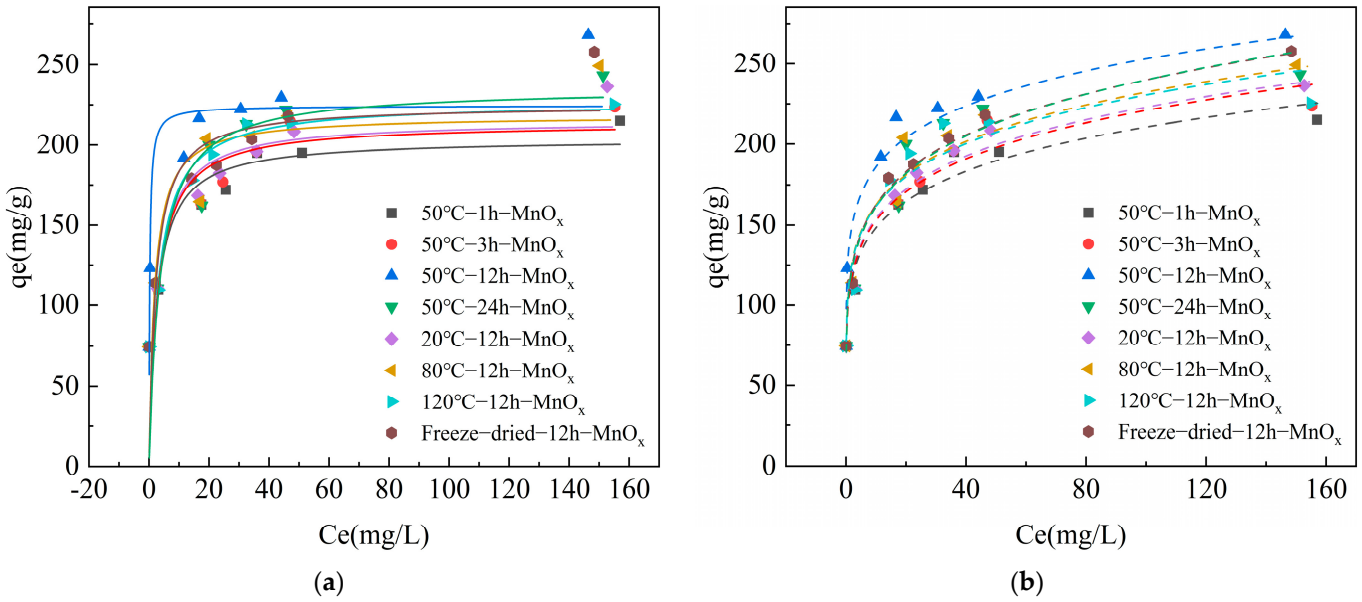

Figure 3. Adsorption isotherms of Mn^{2+} on MnO_x under different drying conditions: (**a**) Langmuir isotherm and (**b**) Freundlich isotherm.

Table 3. Adsorption isotherm parameters of Mn^{2+} by MnO_x under different drying conditions.

Sample	Freundlich Isotherm Model		
	K_F (L/mg)	1/n	R^2
50 °C-1 h-MnOx	104.5 ± 6.70	0.152 ± 0.016	0.948
50 °C-3 h-MnOx	105.6 ± 8.09	0.161 ± 0.020	0.940
50 °C-12 h-MnOx	136.3 ± 9.65	0.134 ± 0.019	0.968
50 °C-24 h-MnOx	108.5 ± 10.8	0.172 ± 0.026	0.943
20 °C-12 h-MnOx	106.6 ± 6.49	0.160 ± 0.016	0.973
80 °C-12 h-MnOx	113.8 ± 10.2	0.154 ± 0.023	0.940
120 °C-12 h-MnOx	113.5 ± 11.3	0.153 ± 0.027	0.959
Freeze-dried-12 h-MnOx	110.4 ± 4.78	0.168 ± 0.011	0.950

The regression coefficient R^2 of the Freundlich isothermal model is higher than 0.9, suggesting that the Freundlich isothermal model can accurately describe the Mn^{2+} adsorption process on MnO_x. The parameter 1/n, which reflects the adsorption kinetic force and potential energy, is inversely related to the adsorption performance, and a smaller 1/n value signifies superior adsorption capacity [31,37]. Thus, it can be concluded that 50 °C-12 h-MnO_x had the best adsorption capabilities for Mn^{2+}.

3.4. Stability and Applicability Analysis of MnO_x for Mn^{2+} Removal

The removal efficiency at 150 min in different reuse cycles was calculated, and the results are shown in Figure 4a. It indicates that, with an increase of the number of reaction cycles, the Mn^{2+} removal efficiency decreased. The highest Mn^{2+} removal efficiency in the sixth cycle was 95.1%. It was obtained for 50 °C-12 h-MnO_x, followed by 50 °C-3 h-MnO_x, 80 °C-12 h-MnO_x, and freeze-dried-12 h-MnO_x, with removal efficiency of 87.8%, 87.3%, and 88.9%, respectively. This suggests that the MnO_x dried at 50 °C for 12 h had the optimal Mn^{2+} removal stability. The Mn^{2+} removal performance of MnO_x in different reuse cycles with the reaction time was also investigated, and the results are shown in Figure S1. It also suggests that 50 °C-12 h-MnO_x has the superior stability in Mn^{2+} removal.

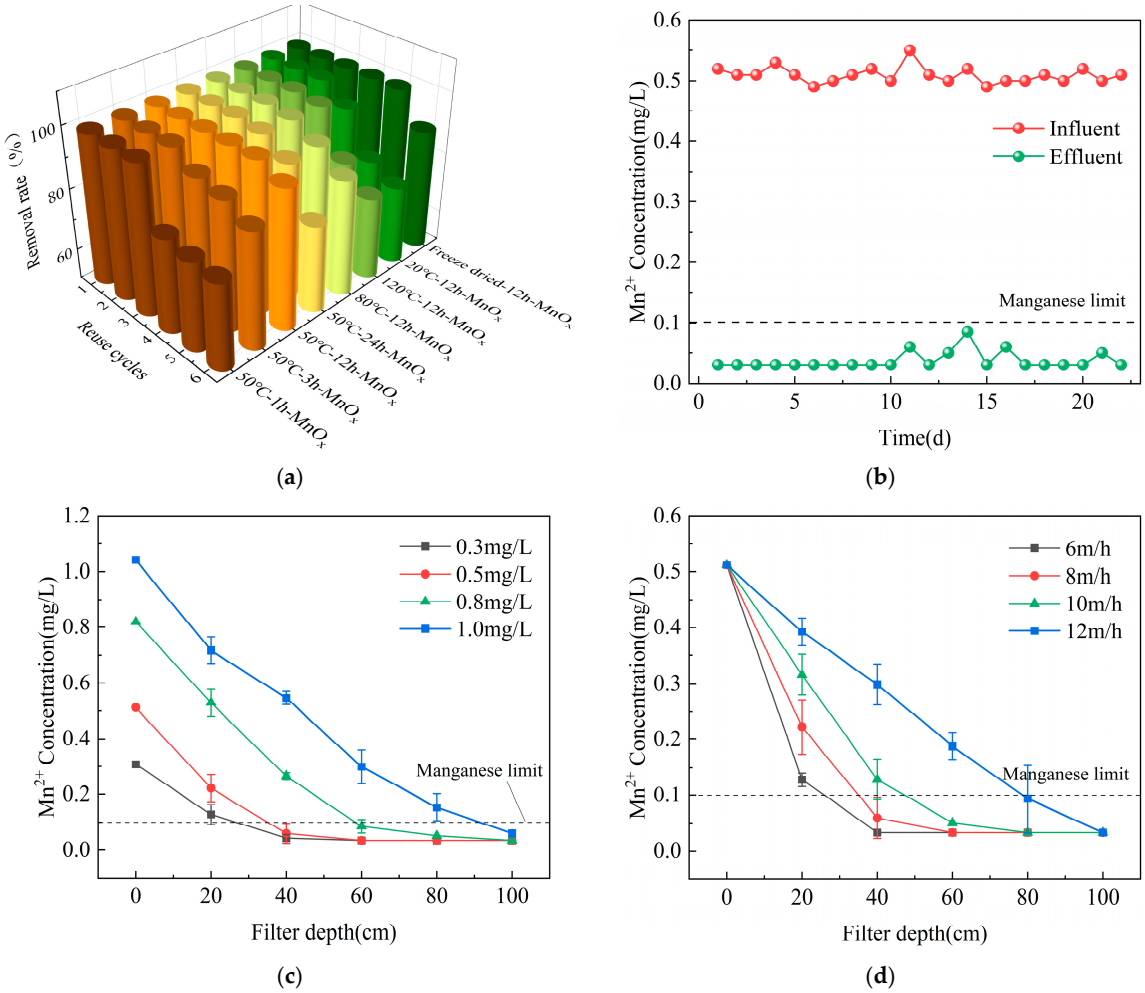

Figure 4. The removal performance of Mn^{2+} by MnO_x in the (**a**) reuse experiments and dynamic filtration test: (**b**) the influent and effluent Mn^{2+} concentrations with time, (**c**) the Mn^{2+} concentration along the filter depth with different influent concentrations, and (**d**) the Mn^{2+} concentration along the filter depth with different filtration rates.

The 50 °C-12 h-MnO_x was coated on quartz sand and a dynamic filtration test was conducted to evaluate the applicability of the MnO_x [32]. The results are shown in Figure 4b–d. This indicated that the Mn^{2+} concentration in the effluent water of the filter column was stably lower than 0.1 mg/L within the operation period of 22 days. When the influent concentration of Mn^{2+} was up to 1.0 mg/L or the filtration rate was up to 12 m/h, the concentration of Mn^{2+} in the effluent water could also meet the drinking water standards. Therefore, it can be concluded that MnO_x has good applicability for groundwater treatment.

3.5. Effects of Drying Conditions on the Structural Characterization of MnO_x

3.5.1. Effects on Morphology

The morphology and the corresponding particle size distribution of the MnO_x treated with different drying operations are shown in Figure 5. It shows that all the samples were composed of nano-sized lamellar particles. The average diameters of the particles on the surface of 50 °C-12 h-MnO_x and freeze-dried-12 h-MnO_x were close, which were 156.6 and 162.2 nm, respectively. Conversely, for 50 °C-24 h-MnO_x and 120 °C-12 h-MnO_x, the size of the particles was smaller. The corresponding average diameters of the particles were 118.9 and 117.1 nm, respectively. Shrinkage deformation was observed, which resulted in a denser surface. These observations suggest that a long drying time or high drying temperature can lead to particle compaction, which may negatively affect the removal of Mn^{2+}.

3.5.2. Thermogravimetric Analysis

The TG and DTG curves of MnO_x dried under different drying conditions are presented in Figure 6. The TG curves demonstrate that MnO_x underwent noticeable weight loss in the drying process. Water in manganese oxides primarily exists in three forms, namely adsorbed water, structural water, and hydroxyl groups [27]. The complete removal of the water molecules in manganese oxides commonly occurs at about 400 °C [35]. Therefore, the weight loss of MnO_x at a temperature lower than 400 °C can be attributed to the decrease in the water content in the oxide. The results reveal that the lowest water content was observed in the freeze-dried-12 h-MnO_x (17.48%), followed by 120 °C-12 h-MnO_x, with water content of 18.55%; the highest water content occurred in 20 °C-12 h-MnO_x (23.06%). This indicates that freeze drying is the most effective method for water removal, followed by 120 °C-12 h-MnO_x. Notably, the water content in 50 °C-24 h-MnO_x was slightly higher than that in 50 °C-12 h-MnO_x, suggesting that extending the drying time at 50 °C has little effect on water removal.

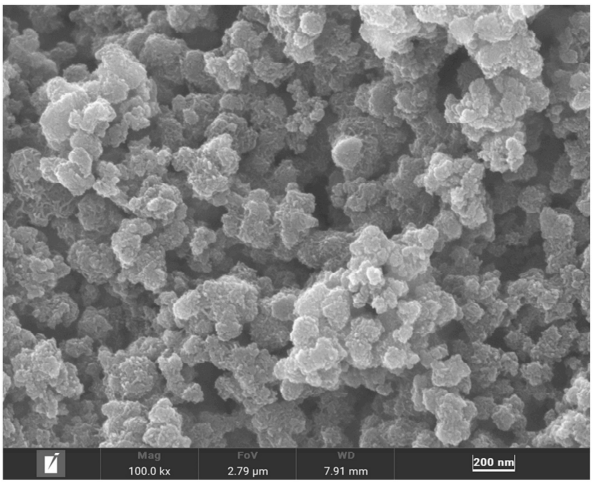

(**a**)

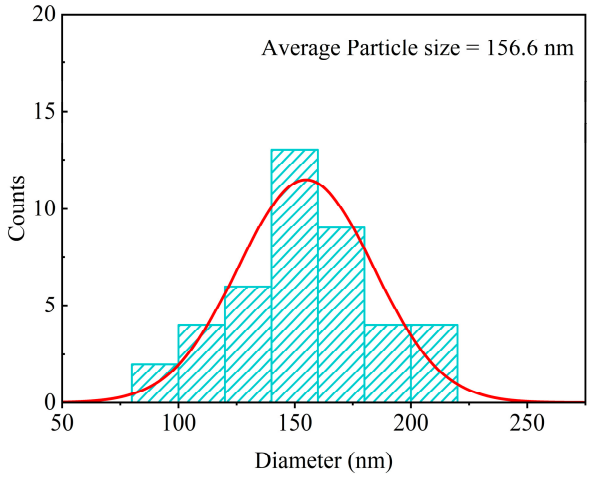

(**b**)

Figure 5. *Cont.*

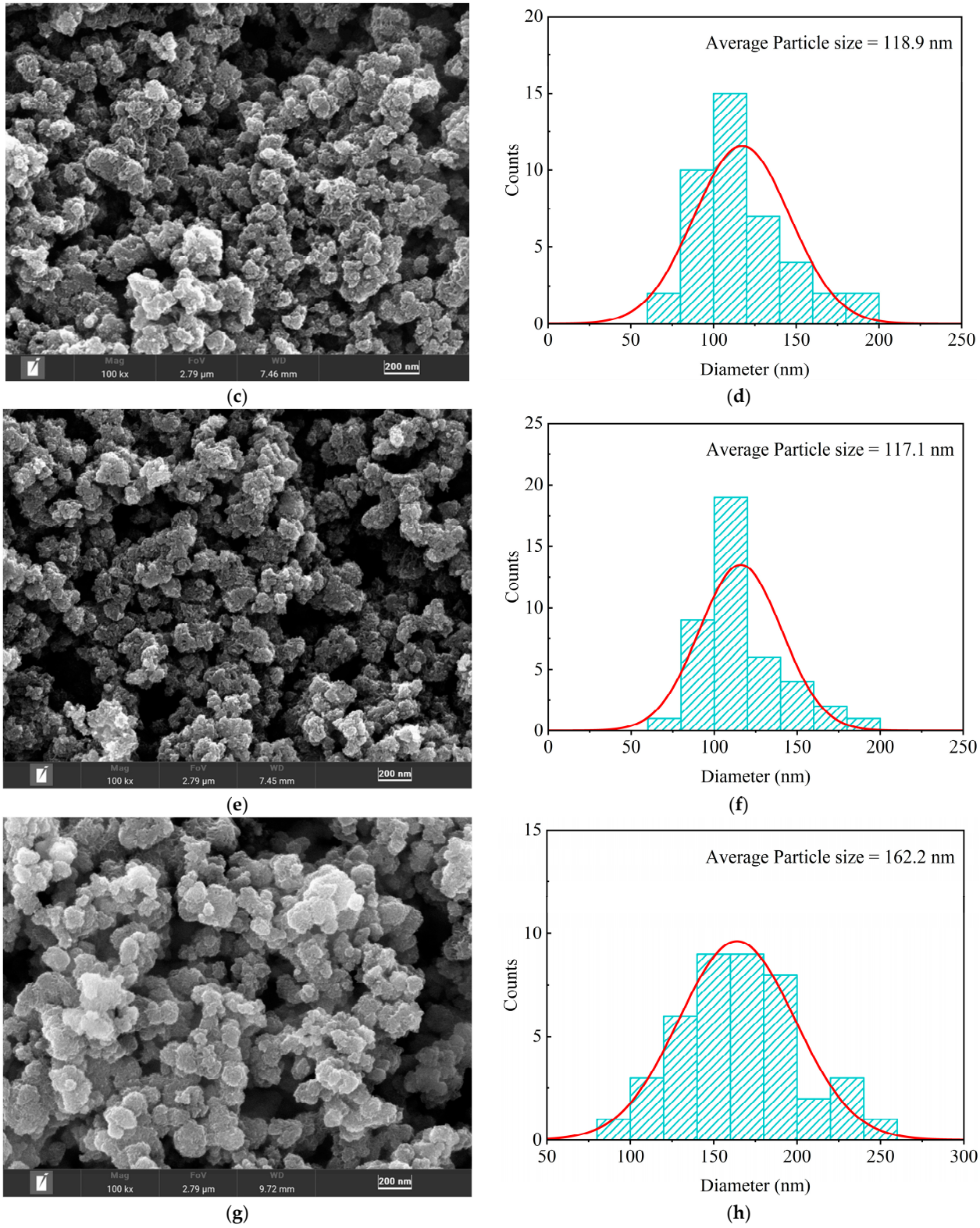

Figure 5. SEM images and the corresponding particle size distributions of MnO_x under different drying conditions: (**a**,**b**) 50 °C-12 h-MnO_x, (**c**,**d**) 50 °C-24 h-MnO_x, (**e**,**f**) 120 °C-12 h-MnO_x, (**g**,**h**) freeze-dried-12 h-MnO_x.

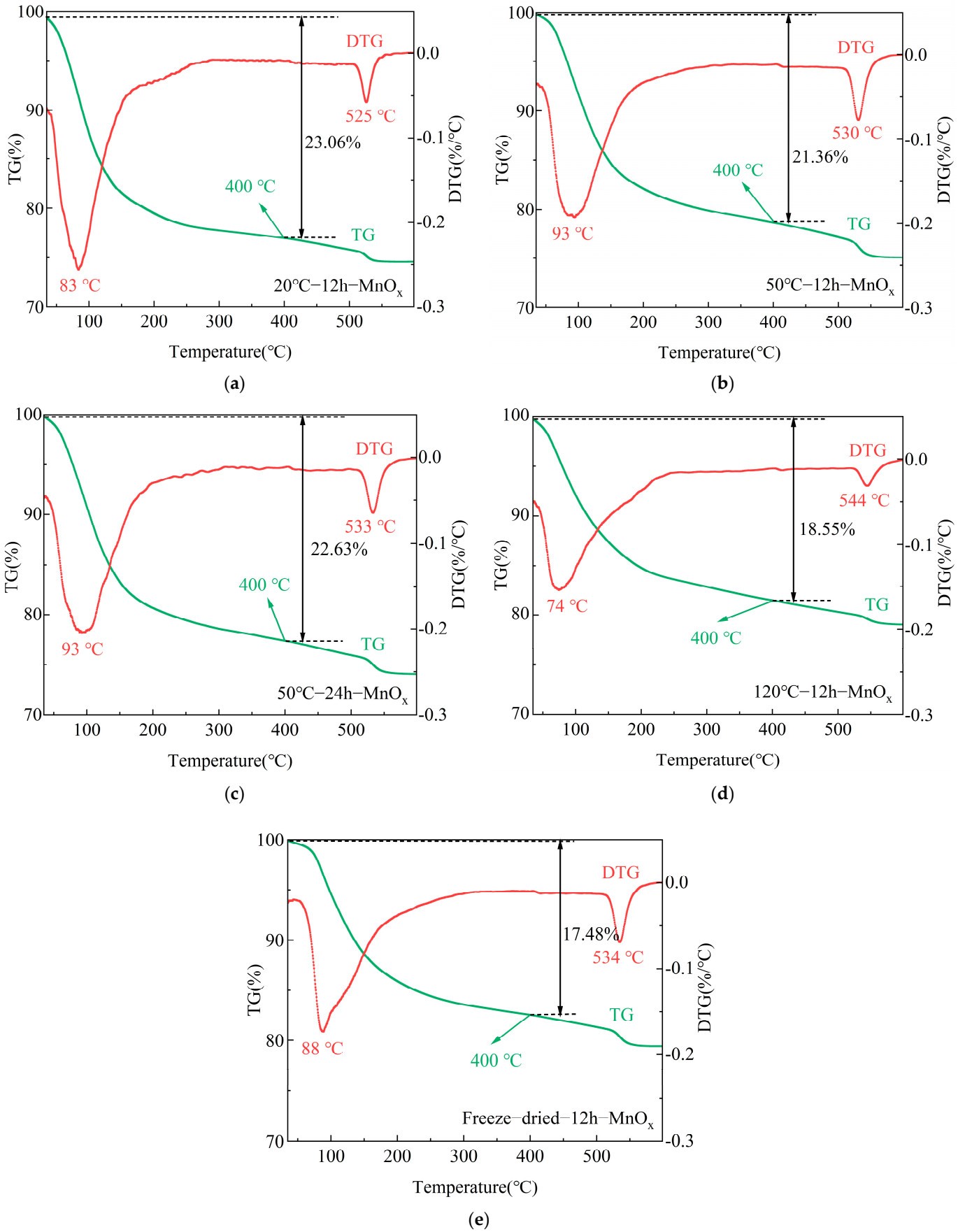

Figure 6. TG-DTG curves of MnO_x under different drying conditions: (**a**) 20 °C-12 h-MnO_x, (**b**) 50 °C-12 h-MnO_x, (**c**) 50 °C-24 h-MnO_x, (**d**) 120 °C-12 h-MnO_x, (**e**) freeze-dried-12 h-MnO_x.

Two significant peaks are observed in the DTG curves. The peak observed in the range of 35–300 °C corresponds to the loss of water molecules from MnO_x. The asymmetry of this peak may be caused by the desorption and reabsorption of the water molecules in the heating process, as well as the overlapping temperature ranges associated with the different water species [24]. Additionally, the right-side tailings of the peak for 120 °C-12 h-MnO_x and freeze-dried-12 h-MnO_x are more obvious, suggesting higher proportions of structural water and hydroxyl groups in these oxides than in the others. The peak observed at temperatures higher than 500 °C is likely due to the loss of lattice oxygen, as well as the phase transition from MnO_2 to Mn_3O_4 [38]. The higher temperature position of the peak corresponds to the lower oxygen activity in MnO_x, which requires more energy for the phase transformation [39]. It shows that when the drying temperature or time increased, the peak position gradually shifted to the right. The most significant shift was observed for the peak at 544 °C in 120 °C-12 h-MnO_x, indicating that the activity of the lattice oxygen in 120 °C-12 h-MnO_x was the lowest.

3.5.3. FTIR and XRD Analysis

The FTIR spectra of MnO_x are shown in Figure S2a. The broad absorption peaks observed between 3000 and 3600 cm^{-1} correspond to the stretching vibrations of adsorbed water molecules on the surface, while the peak at 1630 cm^{-1} is attributed to the bending vibrations of structural water molecules or Mn-OH groups [27]. The absorption peaks in the range of 400–700 cm^{-1} correspond to Mn-O vibrations in MnO_2, which are associated with the deformation of [MnO_6] octahedra [40]. Moreover, these peaks are commonly significant in oxides containing Mn^{3+} and Mn^{4+} and vary among different MnO_x [41]. The peak at 480 cm^{-1} was the most significant in 50 °C-1 h-MnO_x, followed by 20 °C-12 h-MnO_x. Its intensity decreased with a higher drying temperature or longer drying time. The most obvious reductions were observed in 120 °C-12 h-MnO_x and freeze-dried-12 h-MnO_x. Additionally, the intensity of the peak at 1630 cm^{-1}, associated with structural water or Mn-OH groups, was the lowest in 120 °C-12 h-MnO_x compared with the other oxides. The results indicate that the water molecules were the most effectively removed from 120 °C-12 h-MnO_x, followed by freeze-dried-12 h-MnO_x.

The XRD patterns of MnO_x are shown in Figure S2b. Two diffraction peaks of 37.12° and 67.76° were observed across all five samples, with no significant difference. The patterns correspond to Akhtensite-type MnO_2 (ε-MnO_2) [42]. Moreover, the intensity of the peaks was weak, indicating that the MnO_x prepared in this study had low crystallinity, which could provide more adsorption sites and enhance the Mn^{2+} removal [42]. Additionally, a peak at about 24.94° was observed in the patterns of the freeze-dried-12 h-MnO_x and 50 °C-24 h-MnO_x. This can be attributed to α-MnO_2 [25], indicating that a small quantity of α-MnO_2 formed in the 50 °C-24 h-MnO_x and freeze-dried-12 h-MnO_x during the drying process.

3.5.4. XPS Spectra Analysis

The XPS spectra of the Mn 2p and O1s of the manganese oxides are shown in Figure 7. They indicated that the Mn 2p spectra can be fitted into three valence states of Mn(II), Mn(III), and Mn(IV). The corresponding percentages of different species of Mn are shown in Table 4. It can be seen that the percentage of Mn(II) and Mn(III) decreased with the increase in the drying temperature or drying time. In addition, the Mn(III) proportion of 50 °C-12 h-MnO_x was the highest and was up to 60.9%. Since Mn(III) has high reactivity and plays an important role in the oxidation of Mn^{2+} [43], the high removal efficiency of 50 °C-12 h-MnO_x could be attributed to the high Mn(III) proportion. The highest Mn(II) proportion of 46.50% was found in the freeze-dried-12 h-MnO_x. When operating in a

high-vacuum environment, the freeze drying process has little effect on the valence of Mn. Therefore, the composition of the freeze-dried-12 h-MnO_x can be regarded as the initial state of the MnO_x. Thus, it can be found that, in the order of freeze-dried-12 h-MnO_x→50 °C-12 h-MnO_x→50 °C-24 h-MnO_x→120 °C-12 h-MnO_x, the proportion of Mn(II) decreased continually, the proportion of Mn(III) increased firstly and then decreased, and the proportion of Mn(IV) remained unchanged initially and then gradually increased. Consequently, it can be concluded that Mn(II) was first transformed to Mn(III), and then Mn(III) was transformed to Mn(IV) with the increased drying time or drying temperature.

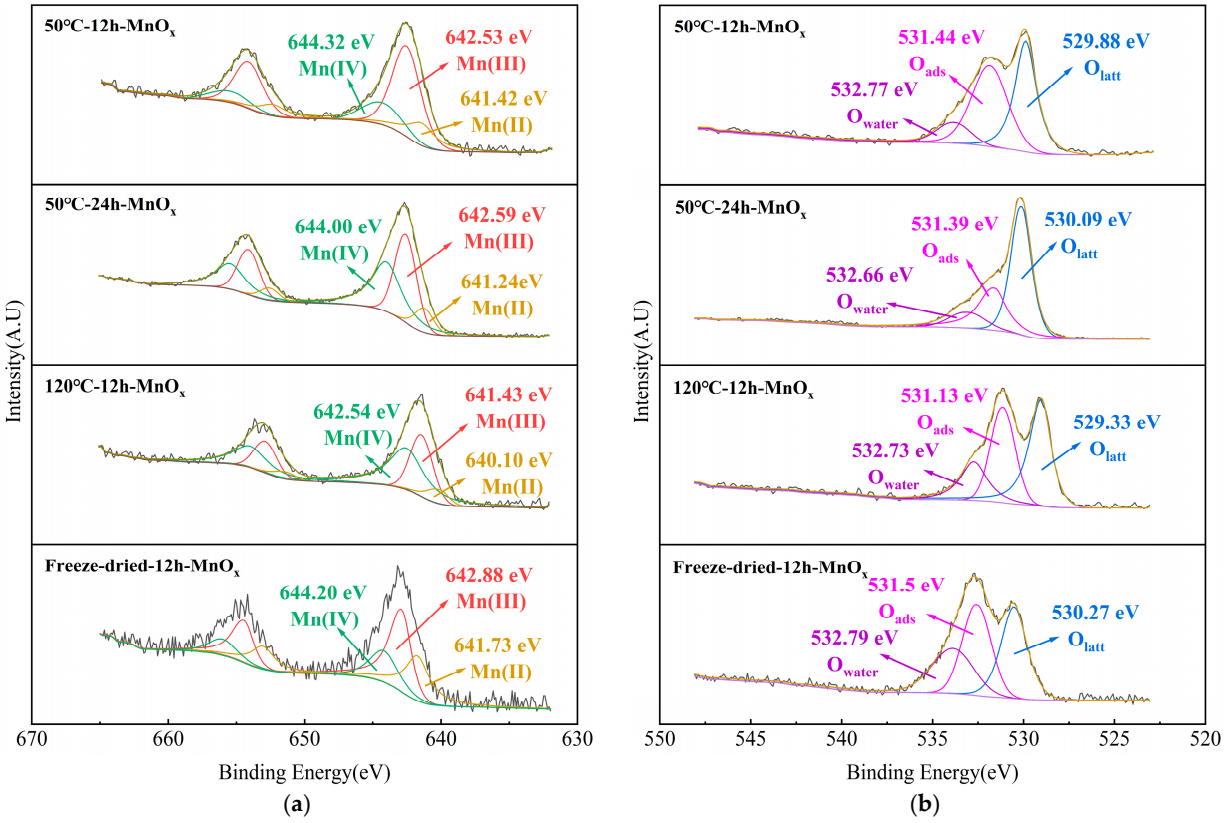

Figure 7. XPS spectra of (**a**) Mn 2p and (**b**) O1s in MnO_x.

Table 4. The percentages of the components of Mn and O based on the XPS spectra.

Sample	Mn $2p_{2/3}$				O1s		
	Mn(II) (%)	Mn(III) (%)	Mn(IV) (%)	Mn(III) /Mn(IV)	O_{water} (%)	O_{latt} (%)	O_{ads} (%)
50 °C-12 h-MnOx	19.60	60.90	19.49	3.12	13.44	40.56	46.01
50 °C-24 h-MnOx	10.92	44.22	44.86	0.98	11.39	54.90	33.70
120 °C-12 h-MnOx	8.78	36.95	54.27	0.68	19.33	45.47	35.20
Freeze-dried-12 h-MnOx	32.94	46.50	20.57	2.26	12.42	34.81	35.60

The molar ratios of Mn(III)/Mn(IV) were also calculated (Table 4). The highest molar ratio of 3.12 was found in 50 °C-12 h-MnO_x and the lowest ratio of 0.68 was observed in 120 °C-12 h-MnO_x. It is known that when Mn(III) is presented on the surfaces of oxides, more oxygen vacancies (V_O) will be generated [44]. The concentration of V_O is positively correlated with the amount of Mn(III) on the surface of MnO_x [45]. Therefore, it can be inferred that the amount of V_O was 50 °C-12 h-MnO_x > freeze-dried-12 h-MnO_x > 50 °C-24 h-MnO_x > 120 °C-12 h-MnO_x. Moreover, the appropriate value of V_O can significantly enhance the reactivity of O in oxides [44], which in turn facilitates the catalytic activity of

MnO_x [46]. This provides a good explanation for the high manganese removal efficiency of 50 °C-12 h-MnO_x.

The XPS spectra of O1s in the manganese oxides are shown in Figure 7b. In the spectra, the peaks at the binding energy of around 530.0 eV can be attributed to the lattice oxygen (O_{latt}) bonded to Mn-O-Mn [47]. The peaks at about 531.5 eV correspond to the surface-adsorbed oxygen (O_{ads}), including O_2^- or O^-, etc. [48], and the peaks at about 532.7 eV are associated with the oxygen in surface-adsorbed water (O_{water}). The content of the surface-adsorbed oxygen was 50 °C-12 h-MnO_x > freeze-dried-12 h-MnO_x > 120 °C-12 h-MnO_x > 50 °C-24 h-MnO_x. The surface-adsorbed oxygen, which is related to the V_O on the surface of MnO_x, plays an important role in the oxidation of Mn^{2+} due to its good mobility [48]. It can also be used to explain the activity change in the oxides.

3.6. Analysis of the Mechanism

3.6.1. The Removal Pathway of Mn^{2+}

The removal performance of Mn^{2+} by different MnO_x with nitrogen or oxygen is shown in Figure 8. In the experiment, the dissolved oxygen (DO) concentration of the reaction solution with O_2 was about 7.53 mg/L, while the DO concentration of the reaction solution with N_2 was lower than 0.15 mg/L. Therefore, the solution with N_2 can be regarded as an anaerobic environment [33]. Mn^{2+} is mainly removed through the adsorption process under the conditions of N_2, and the removal of Mn^{2+} with O_2 occurs via both adsorption and catalytic oxidation. The results showed that the removal rate of Mn^{2+} by MnO_x in an aerobic environment was higher than that in an anaerobic environment, indicating that all oxides had the ability to catalyze the oxidation of Mn^{2+}.

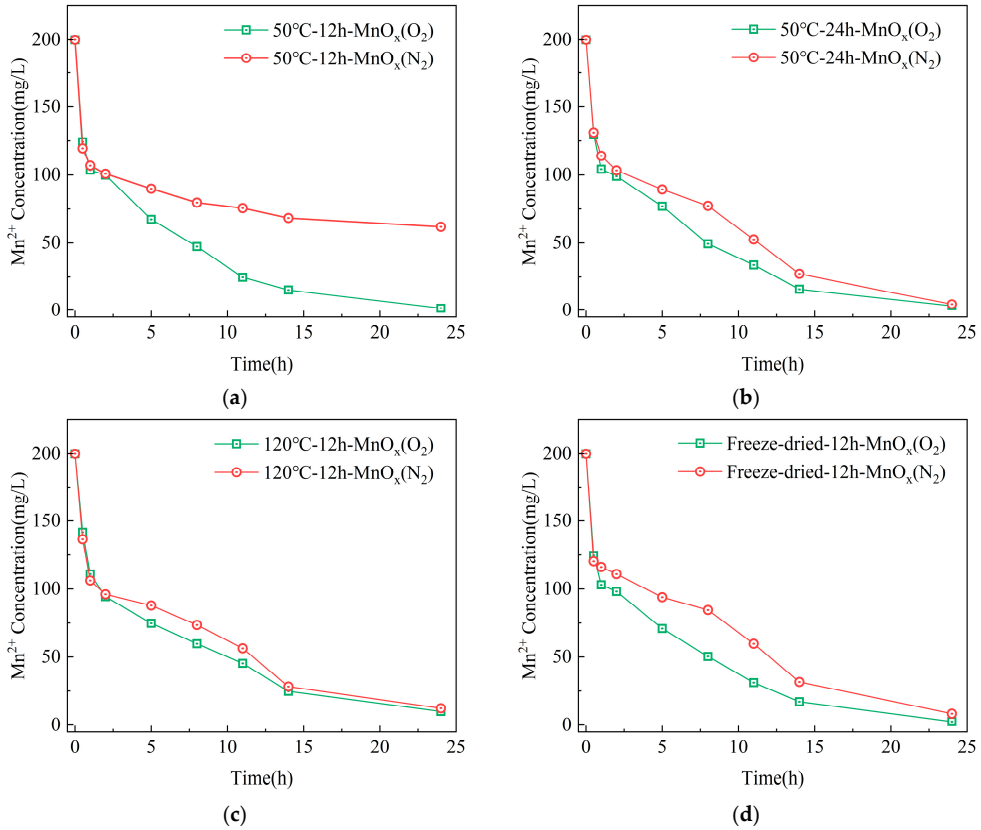

Figure 8. Removal performance of Mn^{2+} by different MnO_x with nitrogen and oxygen: (**a**) 50 °C-12 h-MnO_x, (**b**) 50 °C-24 h-MnO_x, (**c**) 120 °C-12 h-MnO_x, (**d**) freeze-dried-12 h-MnO_x. (MnO_x = 0.2 g/L, Mn^{2+} = 200 mg/L, T = 25 °C, t = 24 h).

However, there was no significant difference in the removal efficiency of Mn^{2+} between 50 °C-24 h-MnO_x, 120 °C-12 h-MnO_x, and freeze-dried-12 h-MnO_x in aerobic and anaerobic environments, indicating that the removal process was dominated by the adsorption process. The removal rate of Mn^{2+} by 50 °C-12 h-MnO_x in an aerobic environment was 99.3%. It was much higher than that in an anaerobic environment (69.1%). This indicates that catalytic oxidation plays an important role in the removal of Mn^{2+} by 50 °C-12 h-MnO_x, which can explain the excellent stability of 50 °C-12 h-MnO_x observed in Figure 4.

3.6.2. XPS Spectra After the Reaction

The XPS spectra of Mn 2p and O1s in the oxides after the reaction are shown in Figure S3. The proportion of Mn(II) on the surface of 50 °C-12 h-MnO_x after reaction in an aerobic environment is much lower than that after reaction in anaerobic environment, indicating that Mn^{2+} can be effectively oxidized by O_2. In addition, the proportion of Mn(II) in 50 °C-12 h-MnO_x after reaction in an aerobic environment is also the lowest among all oxides. This suggests that 50 °C-12 h-MnO_x had the highest catalytic activity for Mn^{2+} oxidation. This result is consistent with that in Figure 8. Compared with the spectra before the reaction (Figure 7), the proportion of Mn(III) in 50 °C-12 h-MnO_x decreased, and the corresponding proportion of Mn(IV) increased, suggesting that the Mn(III) and oxygen vacancies were consumed in the reaction. As shown by the XPS spectra of O1s (Figure S3b), the content of O_{water} on the surfaces of the oxides increased significantly after the reaction, and the corresponding content of 50 °C-12 h-MnO_x was significantly lower than that in the others. It is known that water molecules are preferentially adsorbed at Mn^{2+} sites with an adsorption energy of −16.5 kcal/mol [49]. Thus, the increase in the O_{water} can be attributed to the adsorption of Mn^{2+} on the surface of MnO_x. Additionally, the content of O_{ads} decreased after the reaction, indicating that O_{ads} was involved in the removal of Mn^{2+}.

3.6.3. Summary of the Mechanism

The results indicate that the drying operations had no obvious influence on the adsorption process of MnO_x in a single adsorption experiment, with the adsorption capacity in the range of 110–125.7 mg/g (Table 2). However, it had significant effects on the Mn^{2+} removal efficiency and stability (Figures 1 and 4). Based on the results of the TG-DTG curves (Figure 6) and FTIR spectra (Figure S2a), it can be seen that drying at 120 °C for 12 h and the freeze drying method had the most significant water removal performance. Theoretically, the removal of water molecules can release more active sites on the surface of MnO_x, enhancing the removal of Mn^{2+} [26,34]. However, the removal efficiency and stability of MnO_x dried at 120 °C for 12 h were lower than for that dried at 50 °C for 12 h (Figure 4). Additionally, the structural changes in MnO_x with heat drying and freeze drying were significantly different. The XPS spectra (Figure 7) suggest that, upon increasing the drying temperature or time, the Mn(II) on the surfaces of the oxides will first transform into Mn(III) and then transform into Mn(IV) in the drying process, while the freeze-dried-12 h-MnO_x maintained the highest Mn(II) ratio. The investigation of the removal pathway (Figure 8) confirmed that Mn^{2+} was removed by both adsorption and catalytic oxidation. The XPS spectra of MnO_x after the reaction (Figure S3) suggest that Mn(III) and O_{abs} are critical for the oxidation of Mn^{2+}. Excessive drying reduced the content of Mn(III) and O_{abs} and freeze drying maintained an excessive amount of Mn(II) in MnO_x (Figure 7a), thus resulting in a decrease in the efficiency and stability of Mn^{2+} removal. It can be concluded that the manganese removal capability of MnO_x cannot be assessed merely by the adsorption process; catalytic oxidation is more critical for the Mn^{2+} removal stability. The drying operation can decrease the water content and alter the species of Mn and O, thus affecting the catalytic oxidation of Mn^{2+} by MnO_x.

The process is summarized in Equations (7)–(10). When the MnO_x samples were dried, the adsorption and structural water molecules on the surface could be removed and they released more active sites, enhancing the removal of Mn^{2+} theoretically (Equation (7)). However, the drying operation could also influence the chemical valence of Mn in MnO_x, which would result in different catalytic activity for Mn^{2+} removal. Appropriate drying operations, such as at 50 °C for 12 h, could promote the conversion from Mn(II) to Mn(III) (Equation (8)), and the abundant Mn(III) would oxidize Mn^{2+} effectively (Equation (9)). However, excessive drying operations, such as at 120 °C for 12 h, would lead to the transformation from Mn(III) to Mn(IV), which negatively affects the catalytic oxidation of Mn^{2+}. As catalytic oxidation is more critical for the Mn^{2+} removal stability, appropriate drying operations could enhance the removal performance of Mn^{2+}.

$$MnO_x \cdot nH_2O \xrightarrow{\text{drying}} MnO_x + nH_2O \quad (7)$$

$$Mn(II) \xrightarrow{\text{appropriate drying}} Mn(III) \xrightarrow{\text{excessive drying}} Mn(IV) \quad (8)$$

$$Mn(III) + Mn^{2+} \rightarrow MnO_x + Mn(II) \quad (9)$$

$$Mn(II) + O_{abs} \rightarrow Mn(III) \quad (10)$$

4. Conclusions

In this study, the effects of drying operations on the water properties, structural characteristics, manganese removal performance, and mechanisms of MnO_x were investigated. The results demonstrated that excessive drying time or temperatures led to the shrinkage of the manganese oxide particles, a reduction in surface voids, and a decrease in manganese hydroxyl groups. Conversely, inadequate drying operations resulted in high water content in the oxide, which occupied active sites for Mn^{2+} removal. Additionally, the drying conditions can significantly influence the stability of Mn^{2+} removal by MnO_x. Reuse tests indicated that the sample dried at 50 °C for 12 h exhibited the highest manganese removal stability after six reuse cycles. The removal pathway experiments showed that Mn^{2+} was removed through both adsorption and catalytic processes and the sample dried at 50 °C for 12 h had the strongest catalytic oxidation ability compared with the other samples. The mechanistic analysis revealed that the catalytic oxidation of Mn^{2+} by MnO_x primarily depended on the presence of Mn(III) and adsorbed oxygen on the surface of MnO_x. Higher content of Mn(III) and adsorbed oxygen significantly enhanced the catalytic oxidation of Mn^{2+}. Moreover, freeze drying or inadequate heat drying operations resulted in a large proportion of Mn(II) on the oxide surface, while excessive heat drying operations caused excessive conversion from Mn(II) to Mn(IV), reducing the catalytic oxidation capabilities of the oxides.

Supplementary Materials: The following supporting information can be downloaded at: https://www.mdpi.com/article/10.3390/w17020261/s1, Figure S1: Mn^{2+} removal performance of MnO_x with reuse cycles; Figure S2: (a) FTIR spectra and (b) XRD patterns of MnO_x under different drying conditions; Figure S3: XPS spectra of (a) Mn 2p and (b) O1s of MnO_x after the reaction.

Author Contributions: Conceptualization, R.Z.; methodology, L.Y. and J.Y.; investigation, L.Y. and J.Y.; data curation, L.Y. and J.Y.; writing—original draft preparation, R.Z.; writing—review and editing, R.Z.; project administration, Q.N. and B.Z.; funding acquisition, R.Z. All authors have read and agreed to the published version of the manuscript.

Funding: This work was supported by the Nature Science Basic Research Plan in Shaanxi Province of China (2024JC-YBQN-0548), the Key Laboratory of Membrane Separation of Shaanxi Province (2022MFL01), the Key Research and Development Projects of Shaanxi Province, China [2024SF-YBXM-573], and the Xi'an Municipal Science and Technology Project, China [23GXFW0023].

Data Availability Statement: The data supporting this study's findings are available from the corresponding authors upon reasonable request.

Conflicts of Interest: No potential conflict of interest is reported by the authors.

References

1. Cheng, Y.; Xiong, W.; Huang, T.; Wen, G. Study on the preparation of manganese oxide filter media for catalytic oxidation removal of ammonium and manganese in high alkalinity groundwater: The effect of copper and cobalt doping. *J. Clean. Prod.* **2022**, *366*, 132815. [CrossRef]
2. Fang, K.; Wang, X.; Peng, Z.; Dong, J.; Du, X.; Luo, Y. Gravity driven ceramic membrane loaded birnessite functional layer for manganese removal from groundwater: The significance of disinfection on biofilm. *Sep. Purif. Technol.* **2024**, *332*, 125735. [CrossRef]
3. Shrestha, A.M.; Kazama, S.; Sawangjang, B.; Takizawa, S. Improvement of Removal Rates for Iron and Manganese in Groundwater Using Dual-Media Filters Filled with Manganese-Oxide-Coated Sand and Ceramic in Nepal. *Water* **2024**, *16*, 2450. [CrossRef]
4. Yang, H.; Yan, Z.; Du, X.; Bai, L.; Yu, H.; Ding, A.; Li, G.; Liang, H.; Aminabhavi, T.M. Removal of manganese from groundwater in the ripened sand filtration: Biological oxidation versus chemical auto-catalytic oxidation. *Chem. Eng. J.* **2020**, *382*, 123033. [CrossRef]
5. Ghosh, S.; Mohanty, S.; Akcil, A.; Sukla, L.B.; Das, A.P. A greener approach for resource recycling: Manganese bioleaching. *Chemosphere* **2016**, *154*, 628–639. [CrossRef] [PubMed]
6. Jerroumi, S.; Amarine, M.; Gourich, B. Technological trends in manganese removal from groundwater: A review. *J. Water Process Eng.* **2023**, *56*, 104365. [CrossRef]
7. Dey, S.; Tripathy, B.; Kumar, M.S.; Das, A.P. Ecotoxicological consequences of manganese mining pollutants and their biological remediation. *Environ. Chem. Ecotoxicol.* **2023**, *5*, 55–61. [CrossRef]
8. Mishra, P.; Kaur, L.; Patel, R.; Mishra, R.K.; Verma, D.K.; Daoudi, W. Synthesis and characterization of halloysite-cerium nanocomposite for removal of manganese. *J. Environ. Chem. Eng.* **2024**, *12*, 114611. [CrossRef]
9. Cheng, Y.; Zhang, Y.; Xiong, W.; Huang, T. Simultaneous removal of tetracycline and manganese (II) ions from groundwater using manganese oxide filters: Efficiency and mechanisms. *J. Water Process Eng.* **2021**, *42*, 102158. [CrossRef]
10. Yang, H.; Tang, X.; Luo, X.; Li, G.; Liang, H.; Snyder, S. Oxidants-assisted sand filter to enhance the simultaneous removals of manganese, iron and ammonia from groundwater: Formation of active MnO_x and involved mechanisms. *J. Hazard. Mater.* **2021**, *415*, 125707. [CrossRef] [PubMed]
11. Luo, J.; Zhang, Y.; Chang, H.; Lin, C.; Hu, Y.; Wang, H.; Wang, Y.; Tang, X. Manganese Oxide Enhanced Gravity-Driven Membrane (GDM) Filtration in Treating Iron- and Manganese-Containing Surface Water. *Water* **2024**, *16*, 2374. [CrossRef]
12. Lee, W.S.; Aziz, H.A.; Akbar, N.A.; Wang, M.-H.S.; Wang, L.K. Removal of Fe and Mn from Groundwater. In *Industrial Waste Engineering*; Springer International Publishing: New York, NY, USA, 2023; pp. 135–170.
13. Ducret, J.; Barbeau, B. Modeling Mn(II) autocatalytic sorption on MnO_x-coated filtration media. *J. Water Process Eng.* **2024**, *62*, 105408. [CrossRef]
14. Taffarel, S.R.; Rubio, J. Removal of Mn^{2+} from aqueous solution by manganese oxide coated zeolite. *Miner. Eng.* **2010**, *23*, 1131–1138. [CrossRef]
15. Jin, X.; Fu, J.; Yu, P.; Luo, D. Characterization and properties of manganese oxide film coated clinoptilolite as filter material in fixed-bed columns for removal of Mn(II) from aqueous solution. *Sci. Rep.* **2023**, *13*, 17440. [CrossRef] [PubMed]
16. Zeng, J.; Xie, H.; Zhang, H.; Huang, M.; Liu, X.; Zhou, G.; Jiang, Y. Insight into the effects of oxygen vacancy on the toluene oxidation over α-MnO_2 catalyst. *Chemosphere* **2022**, *291*, 132890. [CrossRef] [PubMed]
17. Li, F.; Yin, H.; Zhu, T.; Zhuang, W. Understanding the role of manganese oxides in retaining harmful metals: Insights into oxidation and adsorption mechanisms at microstructure level. *Eco-Environ. Health* **2024**, *3*, 89–106. [CrossRef]
18. Yang, Y.; Wang, Y.; Li, X.; Xue, C.; Dang, Z.; Zhang, L.; Yi, X. Effects of synthesis temperature on ε-MnO_2 microstructures and performance: Selective adsorption of heavy metals and the mechanism onto (100) facet compared with (001). *Environ. Pollut.* **2022**, *315*, 120218. [CrossRef]
19. Cheng, Y.; Huang, T.L.; Sun, Y.K.; Shi, X.X. Catalytic oxidation removal of ammonium from groundwater by manganese oxides filter: Performance and mechanisms. *Chem. Eng. J.* **2017**, *322*, 82–89. [CrossRef]
20. Xie, X.; Lu, C.; Xu, R.; Yang, X.; Yan, L.; Su, C. Arsenic removal by manganese-doped mesoporous iron oxides from groundwater: Performance and mechanism. *Sci. Total Environ.* **2022**, *806*, 150615. [CrossRef] [PubMed]

21. Yu, P.; Song, Y.; Jin, X.; Fu, J.; Zhang, S. Study on the efficiency of manganese oxide-bearing manganese sand for removing Mn^{2+} from aqueous solution. *Microporous Mesoporous Mater.* **2024**, *364*, 112859. [CrossRef]
22. Junta, J.L.; Hochella, M.F. Manganese (II) oxidation at mineral surfaces: A microscopic and spectroscopic study. *Geochim. Cosmochim. Acta* **1994**, *58*, 4985–4999. [CrossRef]
23. Scheitenberger, P.; Euchner, H.; Lindén, M. The hidden impact of structural water—How interlayer water largely controls the Raman spectroscopic response of birnessite-type manganese oxide. *J. Mater. Chem. A* **2021**, *9*, 18466–18476. [CrossRef]
24. Feng, X.; Cox, D.F. Oxidation of MnO(100) and $NaMnO_2$ formation: Characterization of Mn^{2+} and Mn^{3+} surfaces via XPS and water TPD. *Surf. Sci.* **2018**, *675*, 47–53. [CrossRef]
25. Cai, T.; Liu, Z.; Yuan, J.; Xu, P.; Zhao, K.; Tong, Q.; Lu, W.; He, D. The structural evolution of MnO_x with calcination temperature and their catalytic performance for propane total oxidation. *Appl. Surf. Sci.* **2021**, *565*, 150596. [CrossRef]
26. Zaharieva, I.; Chernev, P.; Risch, M.; Klingan, K.; Kohlhoff, M.; Fischer, A.; Dau, H. Electrosynthesis, functional, and structural characterization of a water-oxidizing manganese oxide. *Energy Environ. Sci.* **2012**, *5*, 7081–7089. [CrossRef]
27. Cheng, Y.; Xiong, W.; Huang, T. Mechanistic insights into effect of storage conditions of Fe-Mn co-oxide filter media on their catalytic properties in ammonium-nitrogen and manganese oxidative removal. *Sep. Purif. Technol.* **2021**, *259*, 118102. [CrossRef]
28. Chaudhry, S.A.; Khan, T.A.; Ali, I. Adsorptive removal of Pb(II) and Zn(II) from water onto manganese oxide-coated sand: Isotherm, thermodynamic and kinetic studies. *Egypt. J. Basic Appl. Sci.* **2019**, *3*, 287–300. [CrossRef]
29. Foo, K.Y.; Hameed, B.H. Insights into the modeling of adsorption isotherm systems. *Chem. Eng. J.* **2010**, *156*, 2–10. [CrossRef]
30. Dutta, D.; Borah, J.P.; Puzari, A.; Valencia, S. Adsorption of Mn^{2+} from Aqueous Solution Using Manganese Oxide-Coated Hollow Polymethylmethacrylate Microspheres (MHPM). *Adsorpt. Sci. Technol.* **2021**, *2021*, 10. [CrossRef]
31. Tang, N.; Niu, C.-G.; Li, X.-T.; Liang, C.; Guo, H.; Lin, L.-S.; Zheng, C.-W.; Zeng, G.-M. Efficient removal of Cd^{2+} and Pb^{2+} from aqueous solution with amino- and thiol-functionalized activated carbon: Isotherm and kinetics modeling. *Sci. Total Environ.* **2018**, *635*, 1331–1344. [CrossRef]
32. Zhang, R.; Yang, S. Rapid start-up and pollutant removal mechanism of MnO_x filter for simultaneous removal of manganese and ammonium. *China Environ. Sci.* **2023**, *43*, 197–205.
33. Lan, S.; Wang, X.; Xiang, Q.; Yin, H.; Tan, W.; Qiu, G.; Liu, F.; Zhang, J.; Feng, X. Mechanisms of Mn(II) catalytic oxidation on ferrihydrite surfaces and the formation of manganese (oxyhydr)oxides. *Geochim. Cosmochim. Acta* **2017**, *211*, 79–96. [CrossRef]
34. Zhou, F.; Izgorodin, A.; Hocking, R.K.; Armel, V.; Spiccia, L.; MacFarlane, D.R. Improvement of Catalytic Water Oxidation on MnO_x Films by Heat Treatment. *ChemSusChem* **2013**, *6*, 643–651. [CrossRef] [PubMed]
35. Dose, W.M.; Donne, S.W. Manganese dioxide structural effects on its thermal decomposition. *Mater. Sci. Eng. B* **2011**, *176*, 1169–1177. [CrossRef]
36. Guo, X.; Wang, J. A general kinetic model for adsorption: Theoretical analysis and modeling. *J. Mol. Liq.* **2019**, *288*, 111100. [CrossRef]
37. Peng, X.; Hu, F.; Huang, J.; Wang, Y.; Dai, H.; Liu, Z. Preparation of a graphitic ordered mesoporous carbon and its application in sorption of ciprofloxacin: Kinetics, isotherm, adsorption mechanisms studies. *Microporous Mesoporous Mater.* **2016**, *228*, 196–206. [CrossRef]
38. Pickles, C.A.; Marzoughi, O. Thermodynamic modelling of decomposition processes in the Mn-O and Mn-O-H systems. *Can. Metall. Q.* **2022**, *62*, 151–170. [CrossRef]
39. Duan, J.; Feng, S.; He, W.; Li, R.; Zhang, P.; Zhang, Y. TG-FTIR and Py-GC/MS combined with kinetic model to study the pyrolysis characteristics of electrolytic manganese residue. *J. Anal. Appl. Pyrolysis* **2021**, *159*, 105203. [CrossRef]
40. Ramarajan, D.; Sivagurunathan, P.; Yan, Q. Synthesis and characterization of sol-processed α-MnO_2 nanostructures. *Mater. Sci. Semicond. Process.* **2012**, *15*, 559–563. [CrossRef]
41. Frey, C.E.; Kurz, P. Water Oxidation Catalysis by Synthetic Manganese Oxides with Different Structural Motifs: A Comparative Study. *Chem.—A Eur. J.* **2015**, *21*, 14958–14968. [CrossRef] [PubMed]
42. Zhang, R.; Yang, S.; Dong, C.; Qiao, Y.; Zhang, J.; Guo, Y. Synthesized akhtenskites remove ammonium and manganese from aqueous solution: Removal mechanism and the effect of structural cations. *RSC Adv.* **2021**, *11*, 33798–33808. [CrossRef] [PubMed]
43. Hu, E.; Zhang, Y.; Wu, S.; Wu, J.; Liang, L.; He, F. Role of dissolved Mn(III) in transformation of organic contaminants: Non-oxidative versus oxidative mechanisms. *Water Res.* **2017**, *111*, 234–243. [CrossRef]
44. Jia, J.; Zhang, P.; Chen, L. Catalytic decomposition of gaseous ozone over manganese dioxides with different crystal structures. *Appl. Catal. B: Environ.* **2016**, *189*, 210–218. [CrossRef]
45. Wang, Z.; Jia, H.; Zheng, T.; Dai, Y.; Zhang, C.; Guo, X.; Wang, T.; Zhu, L. Promoted catalytic transformation of polycyclic aromatic hydrocarbons by MnO_2 polymorphs: Synergistic effects of Mn^{3+} and oxygen vacancies. *Appl. Catal. B Environ.* **2020**, *272*, 119030. [CrossRef]
46. Dong, C.; Qu, Z.; Jiang, X.; Ren, Y. Tuning oxygen vacancy concentration of MnO_2 through metal doping for improved toluene oxidation. *J. Hazard. Mater.* **2020**, *391*, 122181. [CrossRef] [PubMed]
47. Huang, L.; Luo, X.; Chen, C.; Jiang, Q. A high specific capacity aqueous zinc-manganese battery with a ε-MnO_2 cathode. *Ionics* **2021**, *27*, 3933–3941. [CrossRef]

48. Wan, J.; Zhou, L.; Deng, H.; Zhan, F.; Zhang, R. Oxidative degradation of sulfamethoxazole by different MnO_2 nanocrystals in aqueous solution. *J. Mol. Catal. A Chem.* **2015**, *407*, 67–74. [CrossRef]
49. Garcês Gonçalves, P.R.; De Abreu, H.A.; Duarte, H.A. Stability, Structural, and Electronic Properties of Hausmannite (Mn_3O_4) Surfaces and Their Interaction with Water. *J. Phys. Chem. C* **2018**, *122*, 20841–20849. [CrossRef]